

# The Lyman-alpha telescope of the Extreme Ultraviolet Imager on Solar Orbiter

Udo Schühle<sup>\*a</sup>, Jean-Philippe Halain<sup>b</sup>, Stefan Meinig<sup>a</sup>, Luca Teriaca<sup>a</sup>

<sup>a</sup>Max-Planck-Institut für Sonnensystemforschung, Max-Planck-Str. 2, 37191 Katlenburg-Lindau, Germany;

<sup>b</sup>Centre Spatial de Liège, Université de Liège, Liège Science Park, 4013 Angleur, Belgium

## ABSTRACT

On the Solar Orbiter mission, the Extreme Ultraviolet Imager (EUI) set of filtergraph-telescopes consists of two high-resolution imagers (HRI) and one dual-band full Sun imager (FSI) that will provide images of the solar atmosphere in the extreme ultraviolet and in the Lyman- $\alpha$  line of hydrogen at 121.6 nm. The Lyman- $\alpha$  HRI, in particular, will provide imaging of the upper chromospheres/lower transition region of the Sun at unprecedented high cadence and at an angular resolution of 1" (corresponding to a spatial resolution of 200 km at perihelion).

For vacuum-ultraviolet imaging of the Sun the main requirements for the instrumentation are high resolution, high cadence, and large dynamic range. We present here the novel solutions of the instrument design and show in detail the predicted performance of this telescope. We describe in detail how the high throughput and spectral purity at 121.6 nm is achieved. The technical solutions include multilayer coatings of the telescope mirrors for high reflectance at 121.6 nm, combined with interference filters and a multichannel-plate intensified CMOS active pixel camera. We make use of the design flexibilities of this camera to optimize the dynamic range in the focal plane.

**Keywords:** Solar Orbiter, hydrogen Lyman- $\alpha$  line, vacuum ultraviolet, solar telescope

## 1. INTRODUCTION

The Solar Orbiter mission is a joint science mission within the ESA Cosmic Vision Program and NASA Living with a Star Program<sup>[1],[2],[3]</sup>. By approaching close to the Sun and directing its orbit out of the ecliptic plane the Solar Orbiter will provide close-up views of the Sun, in particular its polar regions, and will tune its orbit to the Sun's rotation to allow the spacecraft to observe one specific area for much longer time than possible from an orbit close to Earth. Solar Orbiter is a three-axis stabilized spacecraft equipped with instruments for both in-situ measurements and remote-sensing observations from a highly elliptical orbit approaching the Sun as close as 0.29 AU. After an in-ecliptic phase of perihelion passes where it is nearly co-rotating with the Sun, Solar Orbiter will move the inclination of its orbit to progressively higher heliospheric latitudes, reaching  $\sim 30^\circ$  by the end of its extended mission.

The payload complement of Solar Orbiter contains several in-situ sensors as well as remote sensing telescopes and spectrographs. One set of three imaging telescopes of the remote sensing instrument package is the Extreme Ultraviolet Imager (EUI). Here we present the detailed design and expected performance of the Lyman- $\alpha$  telescope which is one of the three telescopes of EUI.

The hydrogen Lyman- $\alpha$  line at 121.6 nm is the strongest vacuum ultraviolet (VUV) emission line in the solar spectrum and, although optically opaque, it is sensitive to changes in atmospheric structures formed at temperatures typical of the lower chromosphere/upper transition region (about 30000 K). Only few space instruments have been built in the past for imaging the solar outer atmosphere at the hydrogen Lyman- $\alpha$  wavelength. The first cameras were rocket-borne experiments. In 1979 the Transition Region Camera<sup>[4]</sup> made first images of the Sun at a resolution of 1" (corresponding to 725 km on the Sun surface from 1 AU).

---

\* [schuehle@mps.mpg.de](mailto:schuehle@mps.mpg.de); phone 49 5556 979458; fax 49 5556 9796458; [mps.mpg.de](http://mps.mpg.de)

Hoover et al.<sup>[5]</sup> in 1991 acquired full disk images of the Sun at hydrogen Lyman- $\alpha$  with the Multi Spectral Solar Telescope Array (MSSTA) on a sounding rocket flight. These images showed the importance of that emission line for analysis and diagnostics of the structure of the base of the solar atmosphere. However, this line has not yet been systematically exploited through imaging and spectroscopy. Further images have been made with the Transition Region and Coronal Explorer (TRACE) spacecraft<sup>[6]</sup>. However, inadequate suppression of the strong spectral continuum at longer wavelengths up to the visible resulted in images dominated by emission not from the Lyman- $\alpha$  line (low spectral purity)<sup>[7]</sup>.

Spectroscopic imaging and high-resolution spectroscopy of the Lyman- $\alpha$  emission from the solar disk and far out in the corona have been made with the SUMER and UVCS spectrographs on SOHO. Both instruments use their scanning capabilities for building up spectrally pure images of the target areas. However, this technique suffers from the lack of temporal resolution caused by the long scanning times. Fast imaging with very high spatial resolution and good spectral purity has first been achieved with the VAULT instrument<sup>[8],[9]</sup> on a NASA sounding rocket. Recently, the spectral profiles of the Lyman- $\alpha$  line in various regions of the solar disk have been extensively studied by Curdt et al.<sup>[10]</sup> using the SUMER spectrograph on SOHO. VAULT and SUMER results clearly show the diagnostic potential of the Lyman- $\alpha$  line.

## 2. EUI INSTRUMENT OVERVIEW

The design of the EUI instrument package has been presented in a previous paper<sup>[11]</sup>. In [Figure 1](#) we show the structural concept of the EUI sensor unit. Briefly, it consists of one “Full Sun Imager” telescope (FSI) and two “High-Resolution Imager” HRI-EUV and HRI-Ly $\alpha$ . Each telescope is an independent ultraviolet mirror system with specially designed multilayer mirror coatings and spectral filters<sup>[12]</sup>.

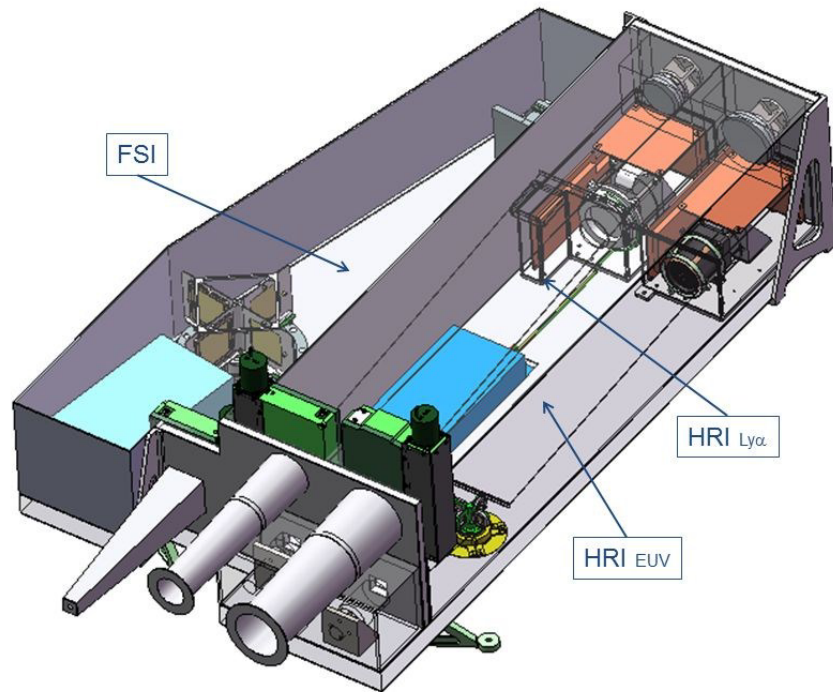


Figure 1. The EUI sensor unit with its three filtergraph telescopes

The performance requirements demand full-Sun imaging at any part of the orbit and high-resolution close-up viewing during scientific observing campaigns.

The Full Sun Imager (FSI):

FSI will provide images of the cold and hot layers of the solar atmosphere along the whole mission orbit. The large-scale corona will be imaged in the spectral bandpass centered at 17.4 nm and dominated by Fe IX/X emission lines formed at temperatures around 0.8–1.1 MK. The lower transition region will be imaged in the 30.4 nm bandpass dominated by the He II emission line formed at a temperature around 0.08 MK (or lower). Simultaneity of images in the two bandpasses is not required for FSI. Both bandpasses can thus be combined inside a single telescope. This is accomplished by a combination of a newly developed multilayer mirror coating optimized for these two bandpasses<sup>[13]</sup> and a filter wheel mechanism located just in front of the focal plane with suitable EUV long pass filters.

The telescope has an aperture of 0.5 cm diameter which allows exposure times between 1 s and 10 s. The field of view is large enough to encompass the full Sun (even if the spacecraft performs off-pointing maneuvers centered on the solar limb near the perihelion of the orbit), namely 5.2 degrees. The spatial resolution corresponds to 1000 km at perihelion (0.29 AU) and 2900 km at the aphelion (0.86 AU). The large field of view is spanned by a detector of 3072x3072 pixels.

The High-resolution imager (HRI):

HRI provides high-resolution imaging of the chromosphere and of the 1 MK corona. The two suitable bandpasses are: H I Lyman- $\alpha$  at 121.6 nm (emission from the upper solar chromosphere/lower TR, at temperatures around 0.03 MK) and from Fe IX/X lines at 17.4 nm (coronal structures at temperatures around 0.8–1.1 MK). The observing periods for the high-resolution imagers include three encounter phases of 10 days during each orbit, centered at the perihelion and around periods of highest northern and southern solar latitudes. During the rest of the orbit high-resolution imagers are not operational.

The effective spatial resolution of the high-resolution imagers is 1" over 2 pixels (i.e., 200 km at perihelion). The corresponding field of view is 0.31 solar radii (with detectors of 2048x2048 pixels). The combination of high cadence and spatial resolution is necessary for the observation of small-scale, highly dynamic events in the solar atmosphere.

### 3. THE LYMAN-ALPHA TELESCOPE OF EUI

Due to the strength of the H I Lyman- $\alpha$  line, it is possible to reach a very high cadence (sub-second) to observe dynamic phenomena in the supergranulation network at the source region of the solar wind and in active regions, as well as cool solar features such as filaments and prominences. The observations in the Lyman- $\alpha$  bandpass should be simultaneous with those in the coronal bandpass. An aperture size of 30 mm allows reaching the observational cadence above 1 Hz.

The Lyman- $\alpha$  channel of EUI will be similar to the EUV HRI design. It is an off-axis Gregory optical system with two mirrors. Spectral band selection will be made by two interference filters and a visible-blind camera. With this design we pursue the goal of a highly efficient filtergraph telescope system with the highest possible throughput and spectral purity by the combination of mirror coatings, two interference filters, and a visible-blind detector with high detective quantum efficiency.

We have computed the expected throughput and spectral purity of the Lyman- $\alpha$  HRI channel for different combinations of filters and mirror coating types. Given the radiance curve of the solar spectrum, the suppression of the strong continuum emission longward of the Lyman- $\alpha$  line is most demanding. With broad band Al/MgF<sub>2</sub> mirror coatings that are highly reflective at VUV and visible wavelengths a high throughput can be achieved. However, with commonly used imaging devices (e.g., lumogen-coated CCDs) that are most sensitive at visible wavelengths, more than two interference filters are necessary, leading to an unacceptable reduction of the throughput. However, a visible-blind detector can be made with a microchannel plate coupled to the sensor array via a fiber optic bundle and a phosphor screen. This way, a spectral purity higher than 90% can be achieved with only two interference filters (still necessary to suppress the UV continuum above 130 nm), a narrow band filter (Acton Research Co. Type 122-XN with a peak transmission of 8%) at the focal plane and a broad band filter (Type 122-N with a peak transmission of 22%) at the telescope aperture, serving also as thermal insulator by reflecting back the visible light.

The throughput of this system can be further improved if a multilayer mirror coating is developed that has a high reflectance at 121 nm and suppresses between 130 nm and 200 nm. In this case, the narrow band filter (122-XN) can also be replaced by a broad band filter (122-N), while keeping the spectral purity well above 90%. Table 1 summarizes the

expected throughput for the optimized coating design and for the baseline Al-MgF<sub>2</sub> coating. Figure 2 gives an idea of the level of details, field of view, and signal level that will be achieved by the HRI Lyman- $\alpha$ .

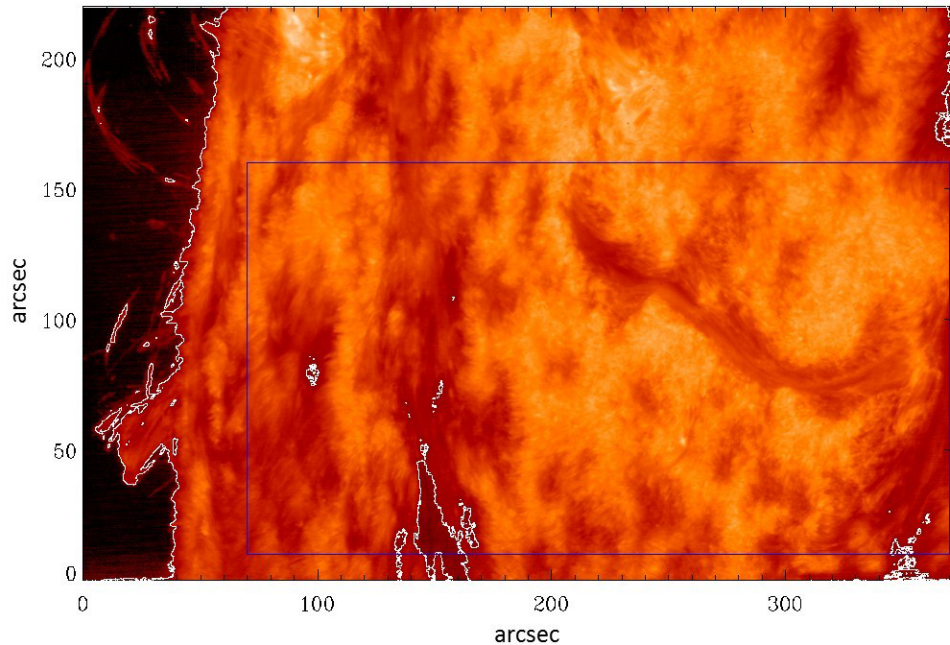


Figure 2. H I Lyman- $\alpha$  image from VAULT-II of an active area near the limb of the Sun. The image has pixel size of  $90 \text{ km} \times 80 \text{ km}$  ( $0.125'' \times 0.110''$  at 1 AU) that is very similar to that of HRI-Ly $\alpha$  at 0.3 AU. The white contours represent the level of 225 detected counts ( $S/N=15$ ) in 1 s in the conservative case of Al-MgF<sub>2</sub> mirrors and a narrow band focal plane filter. The blue box represents the size of half of the HRI-Ly $\alpha$  field of view.

### 3.1 The spectral filters

The spectral band pass will be narrowed by use of commercially available interference filters. Besides rejecting the long wavelength spectrum, it is also necessary to isolate the line of interest (in this case the H I Lyman- $\alpha$  line at 121.6 nm) as much as possible. This is achieved by using interference filters that select a relatively narrow bandpass centered at the wavelength of interest. We chose two interference filters produced by Acton Research Co.. The transmittance of such filters is generally quite low but two filters are assumed to be necessary, one at the entrance of the instrument and one just in front of the detector: a broad band filter 122-N and a narrow band 122-XN, respectively. Note that the narrow filter has lower transmittance than the broad band filter. In addition, the front filter must also withstand the large heat flux from the Sun. To minimize effects due to shifts of the bandpass with temperature, the use of a broad band filter as front filter is foreseen.

Qualifications tests are foreseen. The solar visible and near infrared radiation is producing a heat load on the first optical surface that can only be managed by optical rejection and thermal conductance to space radiators. Last, but not least, the charged particles of the solar wind can have adverse effects on the first surface exposed.

The temperature distribution of the filter will be modeled and thermal-vacuum cycling within the expected temperature range will be performed. Also, since the front filter is the first optical surface that is exposed to the full solar flux, it must be qualified to survive the environmental conditions of the solar orbiter mission. In particular, the high fluence of slow solar wind particles expected during many orbits as close as 0.29 AU is causing a concern. For this reason the irradiation with 1 keV protons, representative for the slow solar wind, will be performed up to a fluence of  $6 \times 10^{17} \text{ cm}^{-2}$ . In addition, the VUV radiation below 180 nm from the Sun with an irradiance of about  $6 \times 10^{13} \text{ photons cm}^{-2} \text{ s}^{-1}$  (averaged over the highly elliptic orbit) will be mostly Lyman- $\alpha$  radiation at 121.6 nm. To investigate any possible aging effect of the filters we perform long-time irradiation tests in our laboratory using a hydrogen Lyman- $\alpha$  lamp (Model HHeLM-L, Resonance Ltd.)<sup>[14]</sup> and a high-intensity krypton lamp (Model KrLM-LHP, Resonance Ltd.) mounted to a vacuum reflectometer (Figure 3).

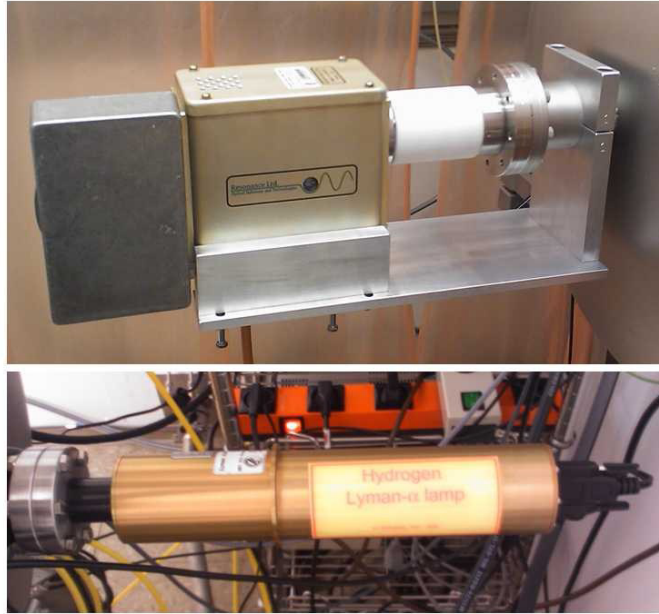


Figure 3. High-intensity krypton lamp and hydrogen line source mounted to a reflectometer vacuum tank for the measurements at 121.6 nm and for the irradiation of samples with 123 nm wavelength.

The Kr-lamp delivers  $3 \times 10^{16}$  photons  $\text{s}^{-1}$   $\text{sr}^{-1}$  and, in our experimental arrangement, creates an irradiance of  $3 \times 10^{13}$  photons  $\text{cm}^{-2}$   $\text{s}^{-1}$  at the position of the sample to be tested. The output is mainly at 123.4 nm which is close enough to Lyman- $\alpha$  wavelength to substitute a hydrogen lamp which would not produce the required intensity.

### 3.2 The mirror coatings

The baseline for the mirror coating is a single Al/MgF<sub>2</sub> layer coating that provides a reflectance at the Lyman- $\alpha$  wavelength of approximately 80%<sup>[15]</sup>, rising to about 90% in the spectral range from 200 nm to the near infrared. This coating is space qualified and, since the mirrors are not directly exposed to the high solar flux, needs no further qualification testing for space flight.

However, spectral purity and throughput can be improved with a special multilayer coating on the two mirrors that is presently under development. The range between 130 nm and 200 nm is the so called "problematic area", where the multichannel plate detector is still sensitive while filters do not sufficiently suppress. With a special multilayer coating design of the two mirrors with high reflectance at 121 nm and suppressing the reflectance between 130 nm and 200 nm the narrow band spectral filter can be replaced with a broad band filter with higher peak transmission. The designed coating, consisting of thin Al and MgF<sub>2</sub> layers, theoretically increases the reflectance at 121 nm and decreases the reflectance in the desired range. The improved mirror coating has a theoretical reflectance of 97.9% at 121.6 nm and an average of 29.5% in the range between 130 nm and 200 nm. Shown in Figure 4 is the calculated reflectance curve of the envisaged coating.

Table 1 compares the expected performance with the two combinations of mirror coatings and filters in regard to signal at typical solar regions to be observed.

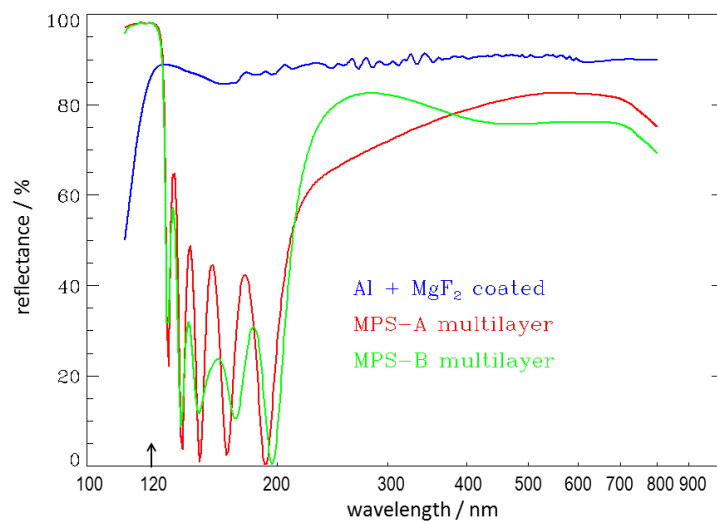


Figure 4. Theoretical reflectance curve of the proposed multilayer mirror coating (two slightly different calculations are shown) compared to an Al/MgF<sub>2</sub> mirror coating<sup>[16]</sup>

Table 1. Expected signal (number of detected photons/pixel/s) of HRI Lyman- $\alpha$  in the case of the baseline (Al-MgF<sub>2</sub>) coating and the optimized multilayer coating design calculated with the spectral radiance of different, representative areas on the Sun.

Target area on the Sun	Baseline coating [MgF <sub>2</sub> ]	Optimized Coating [theoretical]
Coronal Hole	290	1580
Quiet Sun	457	2490
Active Region	1351	7375
Flare [ $\times 10^3$ ]	0.6 – 160 (C – X5 flare)	14 – 870 (C – X5 flare)

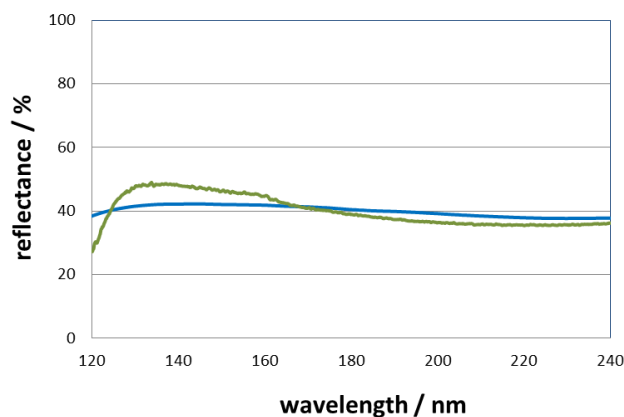


Figure 5. Results of a simplified test coating process: theoretical reflectance (blue curve) and measured reflectance of a mirror sample coating of MgF<sub>2</sub>/Al/MgF<sub>2</sub> (green curve).

Preliminary studies are underway to determine the optimal coating process and the efficiency compared to the theoretical one. As a first step, a simplified coating design study was conducted to test the possibilities of process control in a thermal evaporation coating process. Since the performance of coatings is heavily dependent on process parameters, samples have been produced with a simplified test coating with different process parameters. The test coating was deposited on quartz substrates with a triple layer consisting of 30.5 nm MgF<sub>2</sub>, 9 nm Al und 31.5 nm MgF<sub>2</sub>. The first concern is the controlled evaporation of thin, homogeneous layers of aluminum and magnesium fluoride and to minimize oxidation of aluminum during the process. The results shown in Figure 5 are promising in respect to the agreement between the reflectance results and the theoretical calculation. Although the reflectance at 121 nm is lower than predicted by the model calculation with optical constants, which may be caused by aluminum oxide build-up during the coating process or by absorption of MgF<sub>2</sub>, the results show that production of the thin Al layer is no problem for this coating process. A subsequent study is planned to improve reflectance at 121 nm and to demonstrate feasibility of the manufacturing process of the final mirror coating. The results will be published in a forthcoming paper. Further tests will concentrate on reducing the absorption at short wavelengths and demonstrating reproducibility of the coating process and, finally, environmental tests for space qualification.

### 3.3 VUV detector

The imaging devices for EUI are CMOS active pixel sensors with 2k x 2k format for the HRI channels and 3k x 3k format for the FSI, providing a pixel resolution of 0.5" and 4.5" respectively. The Lyman- $\alpha$  detector will use the same type of sensor and readout electronic circuits but with a "front-side" device while the EUV channels will use back-side thinned devices. For better sensitivity at the Lyman- $\alpha$  wavelength, and for better suppression of solar continuum outside the passband of the filters, the sensor will be mated with an image intensifier that will convert the VUV photons to visible light.

The sensors are under development by CMOSIS (CMOSIS nv, Antwerp, Belgium) and the first prototype devices of 1kx1k format have been delivered. They are presently under functional and performance test<sup>[17]</sup>. Both, back-side thinned and front-side devices are being characterized to select the pixel design that is best suitable for the EUV and the Lyman- $\alpha$  detectors. The test program includes a calibration of the spectral response in the wavelength range from 1 nm to 30 nm and from 40 nm to 240 nm. This will be performed at the Metrology Light Source (MLS) of the Physikalisch-Technische Bundesanstalt (PTB) and the grazing incidence beamline of PTB at the Berlin Electron Storage Ring for Synchrotron Radiation (BESSY II) in Berlin. The spectral response will be measured before and after qualification tests with irradiation by gamma rays, high energy protons and heavy ions, to qualify the devices for the Solar Orbiter mission environment.

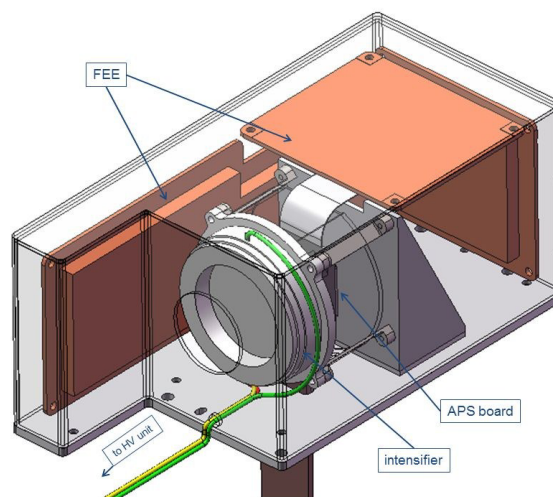


Figure 6. Schematic view of the HRI Lyman- $\alpha$  camera mounted inside a dedicated housing. A separate high voltage power supply box will feed the MCP and anode voltages to the intensifier.

The Lyman- $\alpha$  channel has indeed no metal filters like the EUV channels providing sufficient blocking of visible Sun light. Instead, interference filters are used which need additional visible light blocking. This is accomplished by a blocking filter inside the MCP-intensifier, making it a visible-blind detector. The intensifier is made with a single multichannel plate of 40 mm diameter, with a photocathode coating of potassium bromide (KBr) on the input face of the MCP. The intensifier tube is sealed with an entrance window of magnesium fluoride and a fiber optic output block that carries a "P46" phosphor anode. The output block will be coupled to the sensor by a fiber optic faceplate that is first mounted to the sensor. This produces a 1:1 transfer of the image between the phosphor screen of the intensifier and the sensor device. The sensor board, holding the sensor package, is connected to a cooling strap and, via flexible cable, to the front-end electronics for commanding and data readout. A possible flight configuration is shown in [Figure 6](#).

A breadboard model of such detector has been built and similar units have been successfully tested on NASA rocket experiments<sup>[18]</sup>. Another prototype is under development for mechanical design space qualification. For this purpose, an intensifier unit has been built (by Proxitronic Detector Systems GmbH, Germany) that will be mated with one of the prototype sensors available from CMOSIS. This system (shown in [Figure 7](#)) will be used for laboratory testing.

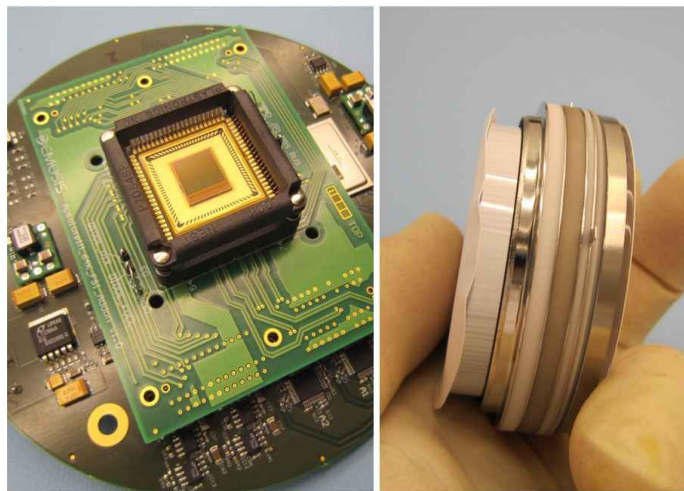


Figure 7. The prototype 1kx1k image sensor mounted in a socket on the electronic test board (left). It will be coupled with the intensifier (right) by a fiber optic faceplate (not shown here) that accounts for the exact sensor geometry.

### 3.4 Aperture Door mechanism

For many reasons, the EUV telescopes have a protective door mechanism at the back-side of the entrance baffle. Among others, the thin metal filters of the EUV telescopes need a protection against pressure differentials during ground and launch operations. In addition, like all UV instruments in space, the contamination with organic material under UV irradiation from the Sun would degrade severely the instrument performance by reducing the optical throughput. The aperture door is thus a necessary protective device.

Each door mechanism can be operated independently to open and close the aperture when required several times during phases of the orbit. For reliability of its operation, it must have a fail-safe, redundant opening device that guarantees the aperture will be open in case of failure of the main driving mechanism. In summary, the aperture doors fulfil the following requirements:

- Provide a contamination barrier during AIV, launch and in-orbit manoeuvres;
- Protect the optical system from UV light during first weeks in space, to allow venting of the instrument without UV light on the optics;
- Protect the instruments during high solar activity and during the non-observing periods;
- Provide a beneficial thermal and radiation protection when closed;

- Independently close and open each EUI telescope.

These requirements can best be fulfilled by sliding doors to be placed in the optical path just in front of the first optical elements, i. e. the entrance filters which are located at the end of the heat-rejecting entrance baffle. To minimize differential pressure on the thin metal filters, they will be mounted as close as possible to the door lid. Figure 8 shows schematically the geometry of this arrangement.

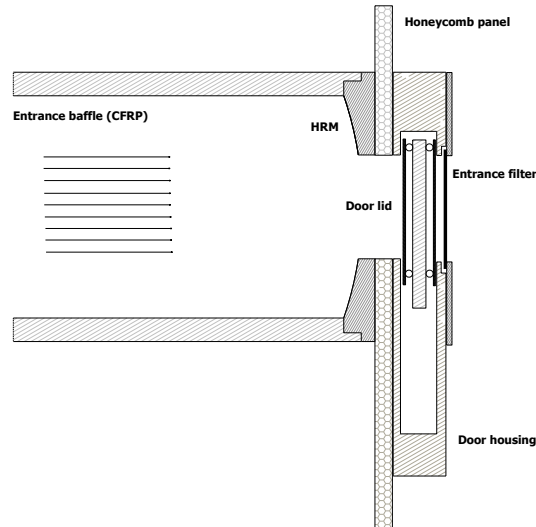


Figure 8. Schematic arrangement of the entrance door mechanism mounted at the heat rejection mirror at the end of the entrance baffle. The entrance filter is mounted on the other side.

The door shall have similar thermo-optical properties as the entrance filter, so as to minimize thermal impact of a change of door position. Although there is no need for vacuum tightness, the sliding door has been designed similarly to a vacuum gate valve such that the door lids can be moved into the optical path and, to complete closure, expands against the housing. The design consists of two door lids on either side of a carriage, moving on two guiding rails. When approaching the closed position, the linear carriage movement stops and changes into expansion. Figure 9 shows one possible design of the mechanism.

The sliding door is operated by a motor drive moving the carriage parallel to the guiding rails. In case of failure of the motor drive, a redundant mechanism can be engaged to decouple this connection and a spring-loaded device moves the door to the open position.

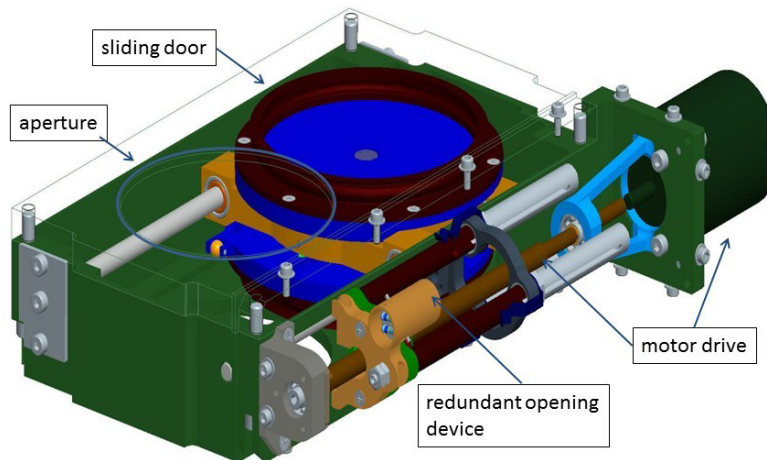


Figure 9. Design of the protective entrance door assembly: a motorized sliding door mechanism with a fail-safe opening device.

## ACKNOWLEDGEMENTS

The EUI instrument is developed in a consortium which includes the Centre Spatial de Liège and Royal Observatory of Belgium (Belgium), the Institut d'Astrophysique Spatiale and the Institut d'Optique (France), the UCL Mullard Space Science Laboratory (United Kingdom), the Physikalisch-Meteorologisches Observatorium Davos (Switzerland) and Max-Planck-Institut für Sonnensystemforschung (Germany).

The Belgian contributions are funded by Belgian Federal Science Policy Office (BELSPO); the French contributions by Centre National d'Etudes Spatiales (CNES), the UK contribution by the UK Space Agency (UKSA); the Swiss contribution is funded through the ESA PRODEX program, and the German contribution by the Deutsches Zentrum für Luft- und Raumfahrt e.V. (DLR). We thank Bernd Chares and Jan Heinrichs of Max-Planck-Institut für Sonnensystemforschung for providing the mechanical design of the entrance door mechanism.

## REFERENCES

- [1] Marsch, E., Marsden, R., Harrison, R., Wimmer-Schweingruber, R., Fleck, B., "Solar Orbiter—mission profile, main goals and present status", *Adv. Sp. Res.* 36, 8, 1360-1366 (2005)
- [2] <http://sci.esa.int/science-e/www/area/index.cfm?fareaid=45>
- [3] <http://science.nasa.gov/missions/solar-orbiter/>
- [4] Bonnet, R. M., Decaudin, M., Bruner, E. C., Jr., Acton, L. W., Brown, W. A., "High-resolution Lyman-alpha Filtergrams of the Sun", *Ap. J.*, 237, L47-L50 (1980)
- [5] Hoover, R.B., Walker, A.B.C., Barbee, T. W., "Solar Observations with the Multi-Spectral Solar Telescope Array", *Proc. SPIE*, 1546, 175-187 (1991)
- [6] Handy, B. N., Bruner, M.E., Tarbell, T.D., Title, A.M., Wolfson, C.J., Laforge, M.J., Oliver, J.J., "UV Observations with the Transition Region and Coronal Explorer", *Sol. Phys.*, 183, 29-43 (1998)
- [7] Handy, B.N., Tarbell, T.D., Wolfson, C.J., Korendyke, C.M., Vourlidas, A., "Calibrated H I Lyman  $\alpha$  Observations with TRACE", *Sol. Phys.*, 190, 351-361 (1999)
- [8] Korendyke, C.M., Vourlidas, A., Cook, J.W., Dere, K.P., Howard, R.A., Morrill, J.S., Moses, J.D., Moulton, N.E., Socker, D.G., "High-Resolution Imaging of the Upper Solar Chromosphere: First Light Performance of the Very-High-Resolution Advanced Ultraviolet Telescope", *Sol. Phys.*, 200, 63-73 (2001)
- [9] Vourlidas, A., Sanchez Andrade-Nuno, B., Landi, E., Patsourakos, S., Teriaca, L., Schühle, U., Korendyke, C.M., Nestoras, I., "The Structure and Dynamics of the Upper Chromosphere and Lower Transition Region as Revealed by the Subarcsecond VAULT Observations", *Sol. Phys.*, 261, 53-75 (2010)
- [10] Curdt, W., Tian, H., Teriaca, L., Schühle, U., Lemaire, P., "The Ly-alpha profile and center-to-limb variation of the quiet Sun", *Astron. Astrophys.*, 492, L9-L13 (2008)
- [11] Halain, J.-P., Rochus, P., Appourchaux, T., Berghmans, D., Harra, L., Schühle, U., Auchère, F., Zhukov, A., Renotte, E., Defise, J.-M., Rossi, L., Fleury-Frenette, K., Jacques, L., Hochedez, J.-F., Ben Moussa, A., "The technical challenges of the Solar-Orbiter EUI instrument", *Proc. SPIE 7732*, 77320R (2010)
- [12] Halain, J.-P., Houbrechts, Y., Auchère, F., Rochus, P., Appourchaux, T., Berghmans, D., Schühle, U., Harra, L., Renotte, E., Zukhov, A., "The Solar Orbiter EUI instrument optical developments", *ICSO Conference* (2010)
- [13] Gautier J., Delmotte, F., Ravet, M. F., Jérôme, A., Bridou, F., Varnière, F., Auchère, F., "Two channel multilayer mirrors for astrophysics", *Opt. Comm.*, 281, 11, 3032-3035 (2008)
- [14] Resonance ltd., 143 Ferndale Drive North, Barrie, Ontario L4N 9V9, [www.resonance.on.ca](http://www.resonance.on.ca)
- [15] Larruquert, J.I., Keski-Kuha, R.A.M., "Far ultraviolet optical properties of MgF<sub>2</sub> films deposited by ion-beam sputtering and their application as protective coatings for Al", *Opt. Comm.* 215, 93-99 (2003)

- [16] Data taken from TRACE secondary mirror Al-MgF<sub>2</sub> coating:  
[http://trace.lmsal.com/Project/Instrument/cal/optic\\_uv/component\\_performance.html](http://trace.lmsal.com/Project/Instrument/cal/optic_uv/component_performance.html)
- [17] A. Ben Moussa, to be published
- [18] Schühle, U., "Intensified solid state sensor cameras: ICCD and IAPS", in [Observing Photons in Space], M. C. E. Huber, A. Pauluhn, J. L. Culhane, J. G. Timothy, K. Wilhelm, A. Zehnder (Eds.), ISSI Scientific Report SR-009, ESA Comm. Div., Noordwijk, NL, ISBN: 978-92-9221-938-3 (2010)